Holographic Wavefront Characterization of a Frequency-Tripled High-Peak-Power Neodymium: Glass Laser (Master's Thesis)

Terrance Jude Kessler

Lab Report 159
September 1984

HOLOGRAPHIC WAVEFRONT CHARACTERIZATION OF A FREQUENCY-TRIPLED HIGH-PEAK-POWER NEODYMIUM:GLASS LASER

by

Terrance Jude Kessler

Submitted in Partial Fulfillment

of the

Requirements for the Degree

MASTER OF SCIENCE

Supervised by Professor James M. Forsyth

Institute of Optics

College of Engineering and Applied Science

The University of Rochester

Rochester, New York

1984

ACKNOWLEDGEMENTS

I extend my thanks to Professor James Forsyth for the many illuminating discussions which provided a context for my research, and for his guidance in maintaining a thesis methodology throughout the course of this study.

I wish to express my gratitude to the personnel of the Laboratory for Laser Energetics for contributing their time, thoughts, and energy in making this thesis project a full learning experience. I especially thank Dr. Wolf Seka for his suggestions and encouragement during my use of the GDL laser system. The GDL operating duo consisting of William Lockman and Raymond Bahr are thanked for the many days and nights of expert operation.

I gratefully acknowledge the financial support from the U.S. Department of Energy Inertial Fusion Project (contract number DE-AC08-80DP40124) and the Laser Fusion Feasibility Project at the Laboratory for Laser Energetics which has the following sponsors: General Electric Company, Northeast Utilities, New York State Energy Research and Development Authority, The Standard Oil Company (Ohio), The University of Rochester, and the Empire State Electric Energy Research Corporation. Such support does not imply endorsement of the content by any of the above parties.

ABSTRACT

Near-field amplitude and phase distributions from a high-peak-power, frequency converted Nd:glass laser (λ = 351nm) have been holographically recorded on silver-halide emulsions. Conventionally, the absence of a suitable reference beam forces one to use some type of shearing interferometry to obtain phasefront information, while the near-field and far-field distributions are recorded as intensity profiles. In this study, a spatially filtered, locally generated reference beam was created to holographically store the complex amplitude distribution of the pulsed laser beam, while reconstruction of the original wavefront was achieved with a continuous-wave laser. Reconstructed near-field and quasi-far-field intensity distributions closely resembled those obtained from conventional techniques, and accurate phasefront reconstruction was achieved. Furthermore, several two-beam interferometric techniques, not practicable with a high-peak-power laser, have been successfully implemented on a continuous-wave reconstruction of the pulsed laser beam.

TABLE OF CONTENTS

LIST OF FIGURES

LIST OF TABLES

INTRODUCTION

The high-peak-power neodymium, glass laser has been extensively developed, primarily for use as a laser driver in Inertial Confinement Fusion (ICF) research. Recent interest in shorter wavelength drivers by the ICF community has resulted in the efficient conversion of infrared radiation (λ = 1.054 μm) to the ultraviolet, third harmonic (λ =351 nm), by means of nonlinear frequency conversion with KDP crystals.[1]

Direct drive ICF, where the confinement time is between 100 ps and 1 ns, is achieved by irradiating spherical fuel pellets with a symmetrical array of overlapping laser beams, and requires a highly symmetric target implosion. A target irradiance uniformity of $\pm$ 1% is believed to be essential in obtaining a sufficiently symmetric fuel compression.[2] The uniformity of laser energy deposition on target has been analyzed using a spherical decomposition of the multibeam interference pattern.[3] The irradiation nonuniformities are understood in terms of two contributing factors from the laser driver. The first factor involves the multibeam geometry, i.e., the number of beams and their orientation, and the energy balance between beams. The second factor involves both the F-number of the focussing lenses and the energy deposition pattern from a single beam, which is determined by the intensity profile of each beam at it's area of contact with the target surface. Therefore, in addition to high peak powers, direct drive ICF requires

that each frequency converted laser beam have a high level of uniformity at the target plane.

Central to the uniformity issue is the need to determine the factors which control the quasi-far-field intensity distribution of the individual beam, and the extent to which they can be manipulated to optimize overall irradiation uniformity. Wavefront measurement techniques, which generate near-field intensity and phase distributions, as well as quasi-far-field intensity distributions of individual laser beams, are essential in fulfilling these objectives. The two near-field profiles, together with a two-dimensional beam propagation code, would constitute a predictive tool for the calculation of the intensity distribution at any given target plane. Furthermore, experimental corroboration would be made possible by the existence of a real time reproduction of the pulsed beam. Figure 1-1 schematically illustrates the relationship between the propagation code predictions and a holographically reconstructed far-field intensity distribution.

Near-field and quasi-far-field intensity distributions, of an infrared (λ = 1.054 μm) high peak power laser (HPPL) beam, have been photographically recorded, while the phase distribution has been measured with shearing interferometry.[2,4] However, photographically recorded focal plane profiles are often invalid (section 2.3), and limited success has been achieved in quantitatively utilizing shearing interferograms. Furthermore, no wavefront measurement techniques have been successfully implemented on the frequency converted HPPL beam (λ = 351 nm).

Wavefront Measurement

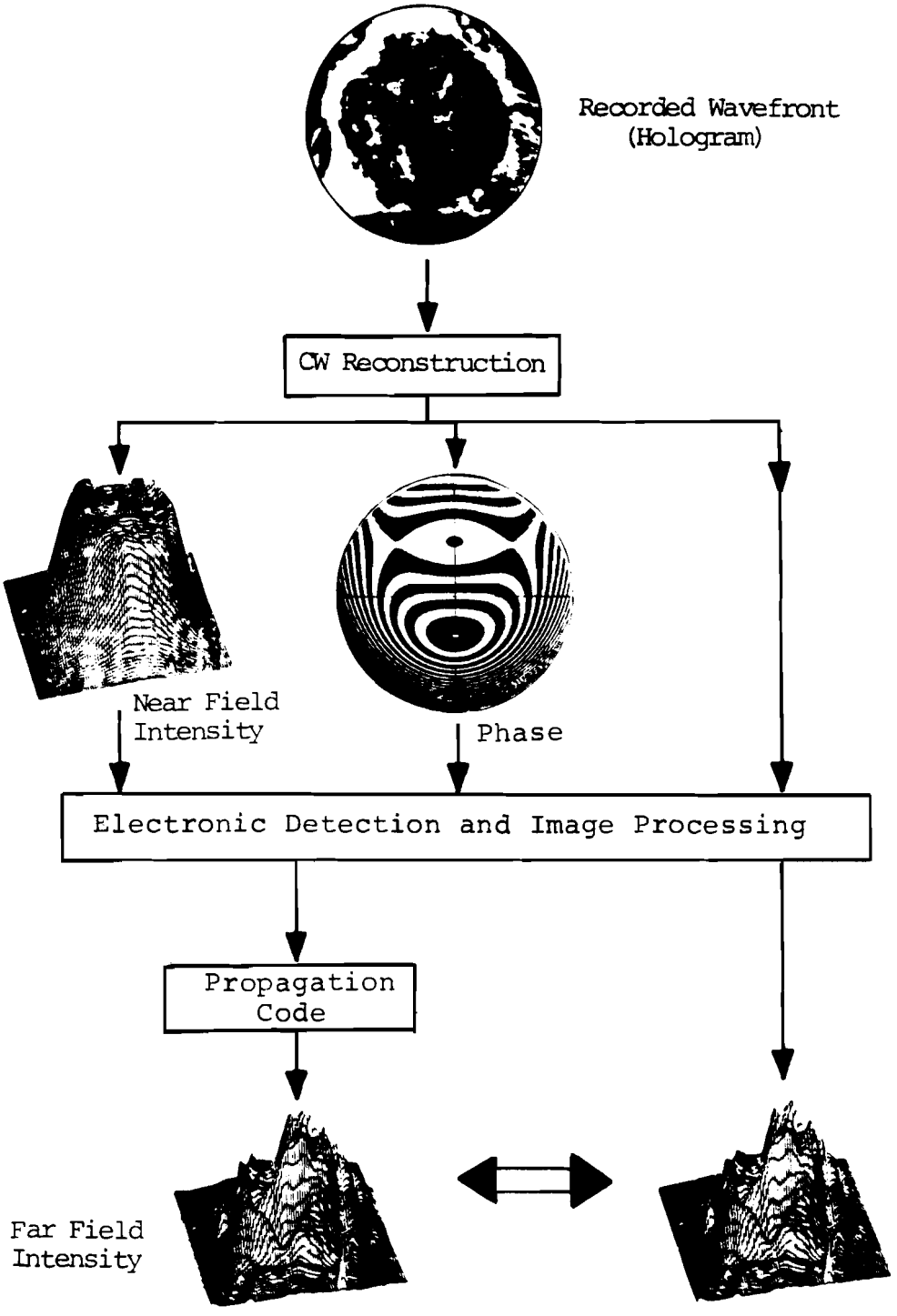

FIGURE 1-1

This thesis is based on the proposition that holographic methods can be implemented on an ultraviolet, frequency converted, high-peak-power laser, in order to obtain a reliable continuous-wave reconstruction for conventional wavefront measurement. Chapter II presents a description of the conventional and alternative wavefront measurement techniques. Chapter III contains a theoretical investigation of the feasibility of producing a locally generated reference beam, for use in holographically recording the wavefront of a HPPL. The demonstration of holographic techniques, and the application of conventional measurement techniques to both the pulsed laser beam and the continuous-wave reconstruction of the pulsed beam are contained in Chapter IV. Conclusions and suggestions for future research compose the final chapter.

REFERENCES

1) Seka W., Soures J.M., Jacobs S., Lund L., Craxton R.S., "GDL: A High Power .35 um Laser", IEEE-J. of Q.E., Sept.'81, Vol. Q.E.-17, #9, p.1689

2) LLE Review, "Uniformity Requirements for Direct Drive Laser Fusion", July'82-Sept.'82, Vol. 12,p.5

3) Skupsky S., Lee K., "Uniformity of Energy Deposition for Laser Driven Fusion", J.Applied Physics, 54(7), July'83 p.3662

4) LLE Review, "Beam Uniformity Measurements on the OMEGA Laser", April'81-June'81, Vol.7,p.5

II. WAVEFRONT MEASUREMENT ALTERNATIVES

2.1 Introduction

A review of the previously used methods to measure the complex amplitude distribution in the near-field and the far-field intensity distribution of a high-peak-power laser (HPPL) is useful in establishing the many practical considerations which influence the final choice of a particular technique. The simplicity of design, operation, and interpretation as well as the versatility, accuracy and cost of the technique must be considered. This review begins with a general inquiry into the pulsed laser wavefront measurement alternatives, which includes useful techniques which have not yet been considered for the set of laser beam parameters (wavelength, pulsewidth, power, etc.) under investigation.

2.2 Phase Measurement

The Lateral Shearing Interferometer (LSI) has been an important tool in the phasefront measurement of the HPPL. This method involves the interference of two identical, but displaced, wavefronts which are derived from, and identical to, the original wavefront. The primary advantage is the fact that the wavefront is interfered with itself, thus eliminating the need for a separate reference wavefront. Figure 2.1 schematically illustrates the physical shear that occurs. The amplitude division of the incident wavefront can be obtained by means of reflecting surfaces, as utilized by the Murty, Bates, and Jamin Interferometers,[1] or by dif-

LATERAL SHEARING INTERFEROMETER

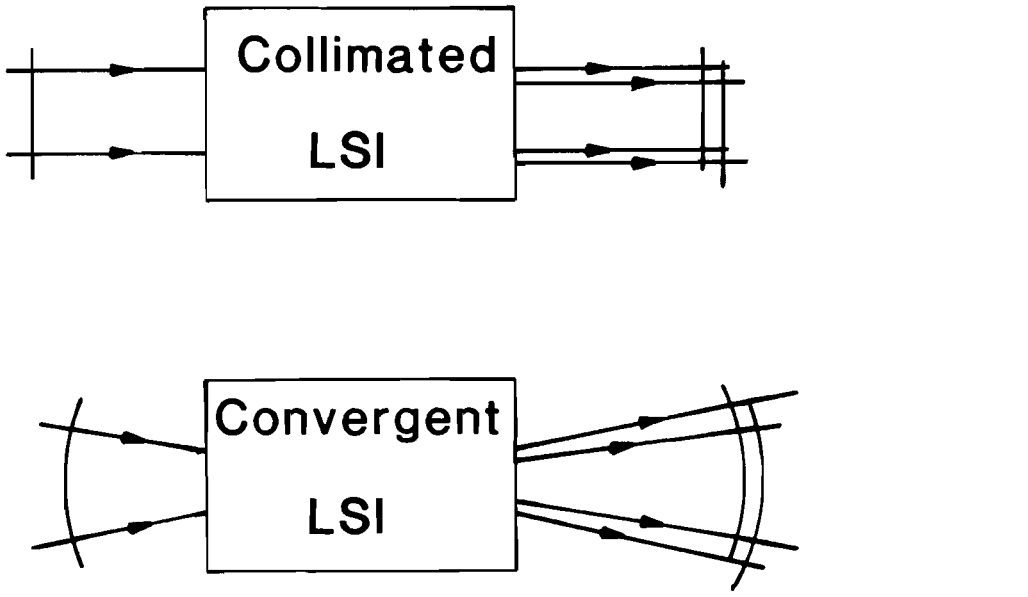

FIGURE 2-1

fraction, as utilized by the double frequency grating lateral shear interferometer.[2]

Referring to Fig. 2.1, the phasefront distribution can be expressed as $W(x,y)$, where x,y are the coordinates of point $P(x,y)$. A shear, $S = \Delta x$, between the two wavefronts introduces a path difference ΔW at point $P(x,y)$ such that $\Delta W(x,y) = [W(x+S/2,y)-W(x-S/2,y)]$. Neglecting constant phase shifts between the two wavefronts, a bright fringe is obtained whenever ΔW is an integer multiple of λ, where ΔW is the average of the wavefront slope $(\partial W/\partial x)$ times the shear distance

$$\left.\frac{\partial W(x,y)}{\partial x}\right|_{\substack{\text{averaged}\\ \text{over } S}} (S) \quad = \quad n\lambda \tag{2-1}$$

The fringes of the lateral shear interferogram represent loci of constant wavefront slope, averaged over the shear distance.[3] The recovery of $W(x,y)$ is improved by a knowledge of the wavefront slope in two orthogonal directions, unless rotational symmetry is assumed. A second interferogram, where the shear direction is along the y axis, must be obtained in this case.

Given a nominally collimated wavefront, the Murty plane parallel plate interferometer (see Fig. 2.2) is a relatively simple method of acquiring wavefront slope information. The two interfering wavefronts are composed of front and rear surface reflections which are sheared according to the following equation,

MURTY INTERFEROMETER

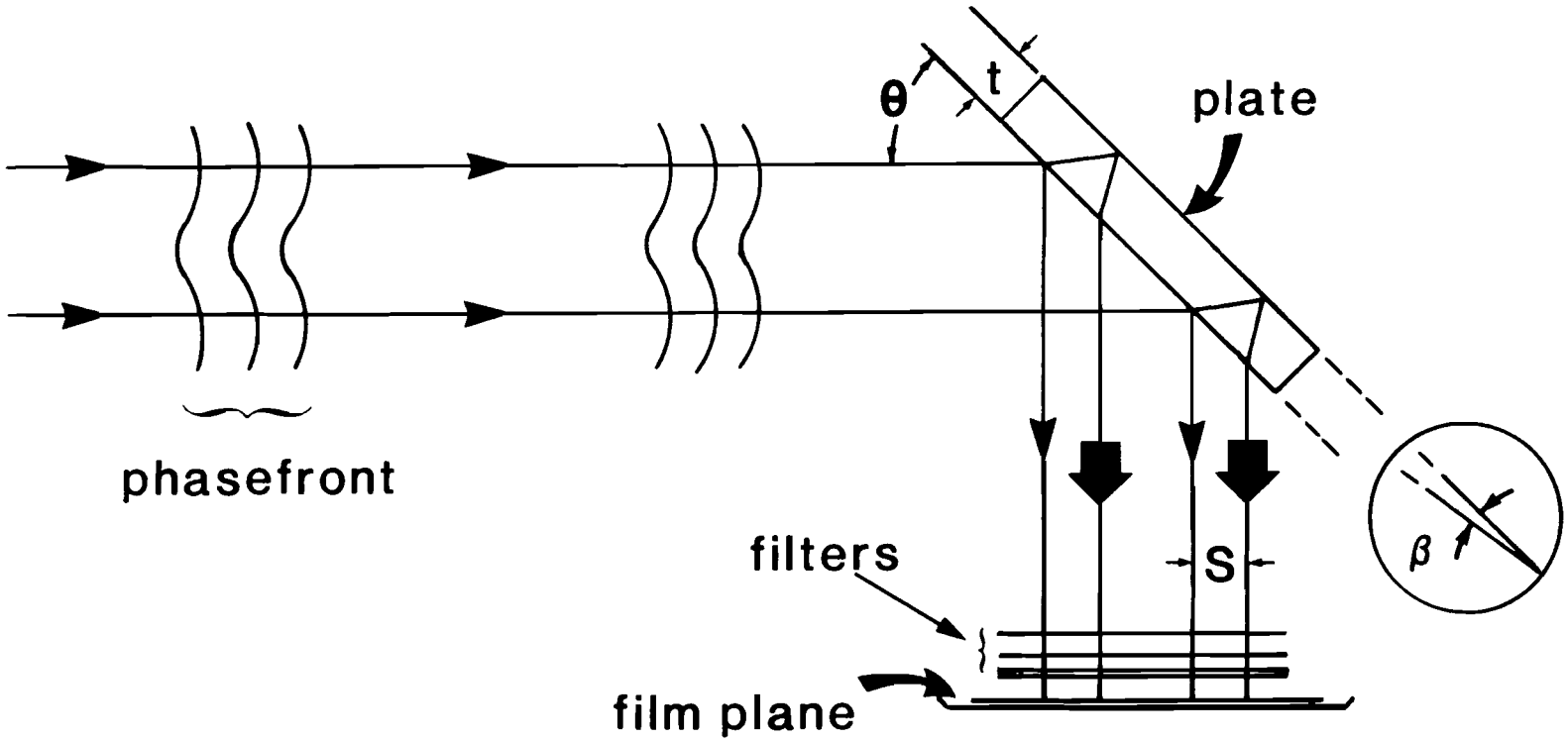

FIGURE 2-2

$$S = \frac{(t)\sin(2\theta)}{(n^2 - \sin^2\theta)^{\frac{1}{2}}} \qquad (2\text{-}2)$$

were t is the plate thickness, n is the refractive index and θ is the angle of incidence. The corresponding optical path difference between the two wavefronts is given by,

$$OPD = 2t(n^2 - \sin^2\theta)^{\frac{1}{2}} \qquad (2\text{-}3)$$

For an uncoated plate, the magnitudes of the two reflections are equal, and determined by the Fresnel reflection coefficients, thus insuring high fringe visibility for a sufficiently coherent source. The sensitivity is dependent upon the shear distance and any tilt introduced between the two reflecting surfaces. Generally tilt is introduced in the direction orthogonal to that of the lateral shear. In the case of shear in the x direction, the optical path difference associated with the tilt may be represented as a linear function of the y coordinate,

$$\Delta W = Ay = n\lambda \qquad (2\text{-}4)$$

where A is the tilt angle, λ is the wavelength of light and n is the refractive index. In the absence of any aberrations, this equation represents a system of straight fringes parallel to the x axis.

In the case of a wavefront with large, multiple aberrations, any tilt would further complicate analysis. A wavefront which is roughly charac-

terized, and known to have small aberrations of a particular type, requires tilt fringes for interferometric reduction since it is easier to evaluate the modulation of nominally straight fringes than to evaluate an almost complete absence of fringes.

Several methods of obtaining two orthogonal wavefront slopes are available. A single plate can be used in two different orientations if the wavefront in two consecutive experiments is reproducible. The use of two plates, orthogonally oriented, is a more expensive solution when simultaneity is a requirement. The double frequency grating is another solution; two shears are obtained by one holographic, double frequency, crossed, diffraction grating. The amount of shear is determined by the difference between the two spatial frequencies which make up the crossed grating. An important advantage to this technique, as opposed to the Murty interferometer, is that no optical path difference (time differential) between the sheared wavefronts exists. Therefore, any temporal incoherence effects in a pulsed beam will not blur the fringe pattern. Fringe blurring would be attributable to time dependent phase changes during the pulse, since a photographic recording device time-integrates the interference pattern.

Shearing interferometry has an inherent disadvantage over conventional wavefront interferometry because of the amount of analysis required to obtain the original wavefront. The most common analytical procedure assumes that the unknown wavefront $W(x,y)$ is a smooth function that can be represented by a two dimensional polynominal. The polynomial coefficients are calculated using a least squares fitting of the wavefront slope values obtained from the measurement of the fringe positions. Rimmer and Wyant state that the accuracy of the final results can

be as good as the accuracy of the measured data.[4] They point out that the major sources of error in their results are the measurement of the shear value and the polynomial fit to the data. They claim an error as small as .04 wavelength RMS has been obtained in the measurement of a wavefront with about one wavelength of aberration. However, an actual attempt at analyzing the data obtained from a HPPL points out the practical difficulties and enormity of the task.[5]

Figures 2.2 and 2.3 schematically illustrate the type of set up that each method requires for use on a HPPL. The Murty design utilizes a combination of wedged reflectors and attenuating filters to insure proper exposure of the photographic record. Figures 2.3 shows the actual setup used to obtain grating-shearing interferograms on an infra-red HPPL. By placing the grating near the focus of the lens system, lateral shearing interferograms are produced on either side of the zero order and in two orthogonal directions. An obstruction which blocked the zero order light was placed ahead of the final lens, to preserve the fringe visibility in the $\pm$ 1 diffracted orders. High visibility interference fringes were obtained on one beam from a twenty-four beam laser system (OMEGA) on a regular basis, but high power densities on the holographic grating resulted in occasional damage.[6] Although the results offered increased understanding of the beam performance in the focal spot as a function of the aberrations in the beam, an accurate analysis of the fringes was never completed.

The point diffraction interferometer (PDI)[7,8] is another potential tool for use on the HPPL. The PDI is basically a two-beam, common-path interferometer in which the reference beam is generated by the diffraction from a small aperture in a partially transmitting material. The

DOUBLE FREQUENCY GRATING

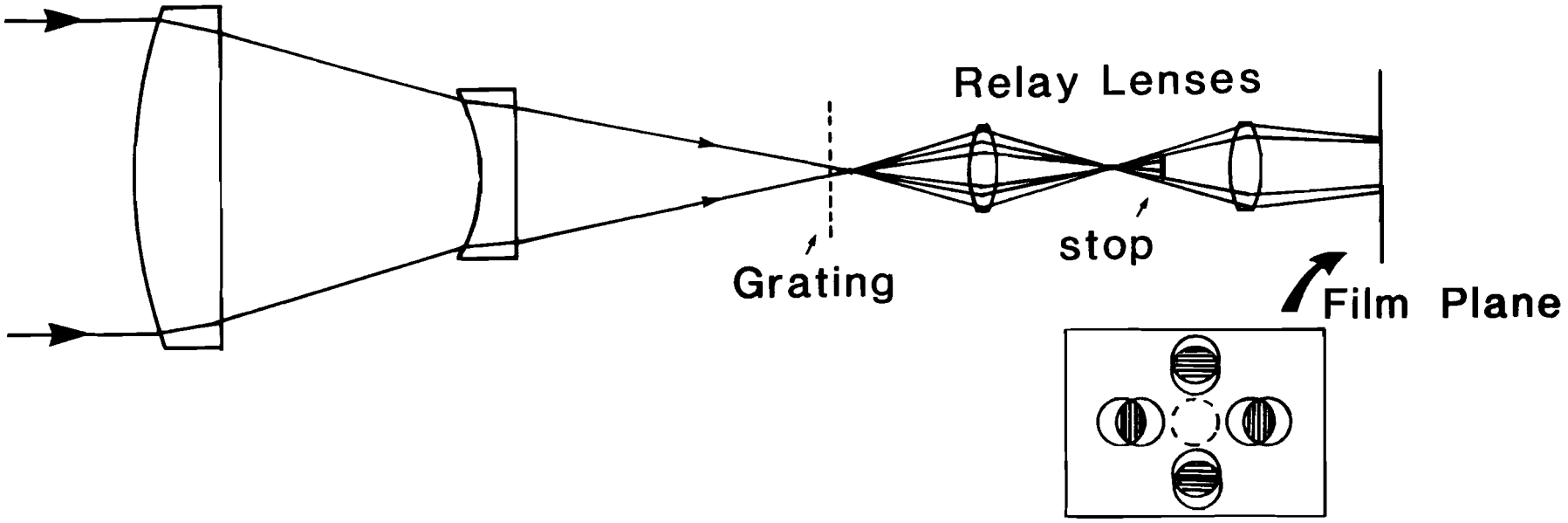

FIGURE 2-3

material, either a thin film deposited on a substrate, or a bulk absorption plate, is placed at the Fourier transform plane of a focussed wavefront as shown in Fig. 2.4. The pinhole is positioned so that some portion of the aberrated point spread function of the wavefront is diffracted into a perfect spherical wave reference beam. The attenuation coefficient of the material is chosen so that high visibility fringes result from the interference of the two wavefronts. The fringe quantity and shape can be chosen by adding or substracting tilt and defocus by laterally and logitudinally displacing the PDI, respectively. The disadvantage of the PDI is that these adjustments also affect the fringe visibility since the reference beam depends upon the intensity distribution of the aberrated point spread function. Unlike lateral shearing interferometry, the fringes from a PDI interferogram trace out contours of regions of equal optical path difference. A map of the wavefront phase is obtained directly.

An infra-red Smartt Interferometer has been successfully designed and used to measure the phase of a CO_2 HPPL.[9] High power densities exclude any type of interferometer which focusses the light onto a coated surface, since a vaporization of the thin film coating, used to attenuate the wavefront, usually occurs. This new design utilized a substrate consisting of a 13 micron thick, epitaxially grown, silicon section into which a high conductivity n-type dopant is driven in by means of a diffusion process. To avoid high power densities on the surface, high F/# systems were used in conjunction with a 40 micron diffraction aperture, along with an initial attenuation of the full beam. The trade offs were found to be between the choice of aperture size and wavefront attenuation versus the contrast and accuracy of the fringes. A peak to valley error of $\lambda/20$ was obtained (λ =10.6 μm).

POINT DIFFRACTION INTERFEROMETER

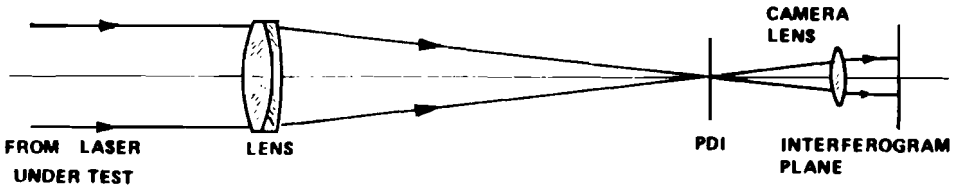

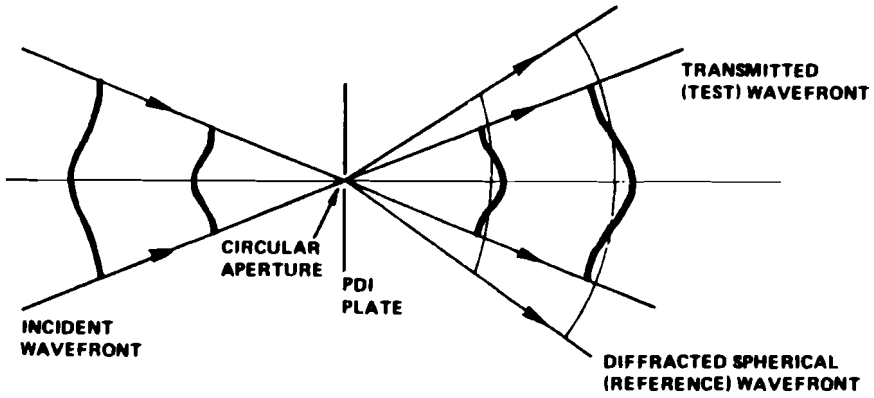

FIGURE 2-4

A variation of the Mach-Zehnder Interferometer has been used to measure the beam parameters of a continous-wave HeNe gas laser.[10] In Fig. 2.5, a TEM_{00} mode laser beam is used as a signal beam. A reference beam is obtained by enlarging the signal beam sufficiently to produce a plane wave with uniform amplitude. Direct measurements of the resulting interferogram and intensity distribution were made to obtain beam parameters.

Holographic techniques allow the possibility of recording and subsequently reconstructing the amplitude and phase of a wavefront. Conventional holographic interferometry involves the storage of two or more temporally separated wavefronts, and an interferometric comparison between them is made during reconstruction. Alternately, the wavefront reconstructed by diffraction at the hologram can be made to interfere with another wavefront transmitted through the hologram. In this case, real time, two-beam type fringes are obtained. Generally this is applied to vibrational analysis or mechanical stress measurement, where the two interfering wavefronts are both object wavefronts and time dependent phase changes are studied. When a plane wave is used as the interfering wavefront transmitted through the plate, then the phase of the object wavefront itself can be visualized in terms of two-beam interference fringes. A hologram of a pulsed laser can be recorded with a locally generated reference beam from the pulse itself.[11,12] The object wavefront can be subsequently reconstructed with an appropriate continous wave laser. Like the PDI, this interferometric technique directly produces wavefront information.

MACH-ZEHNDER INTERFEROMETER

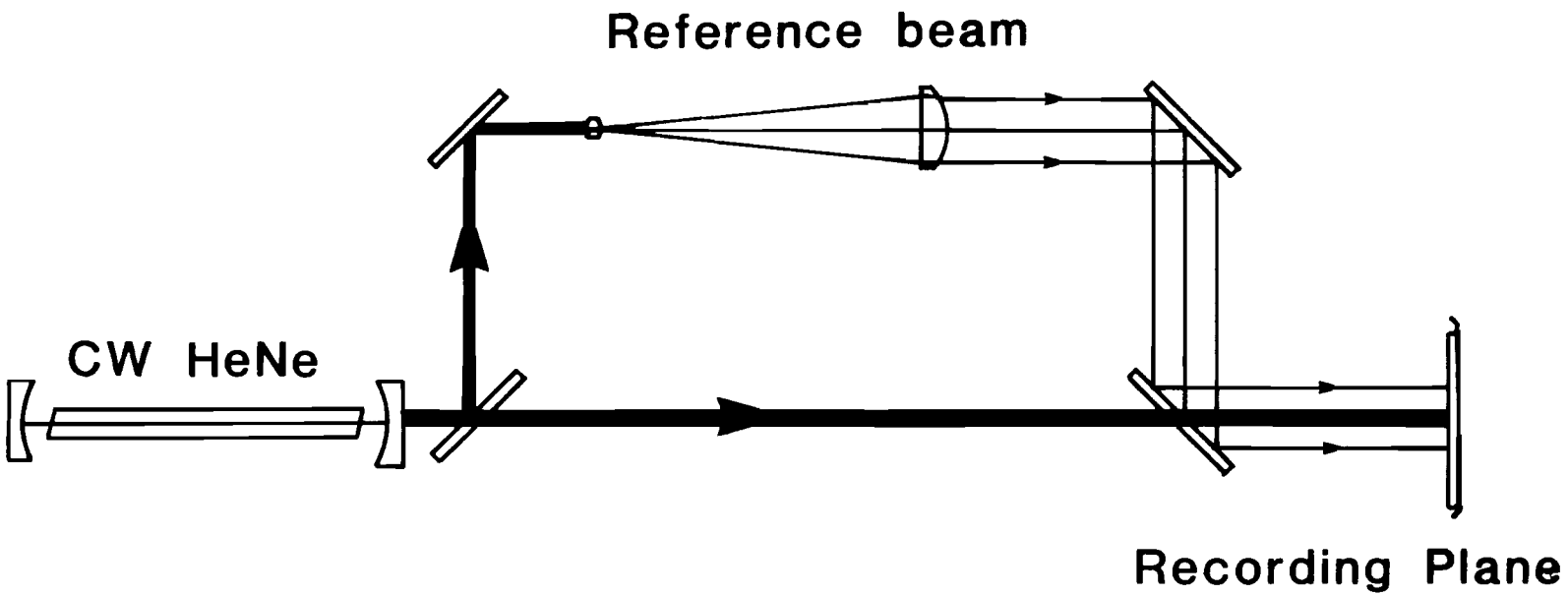

FIGURE 2-5

2.3 Intensity Measurement

Many techniques are available in recording the near-field intensity distribution of a HPPL. The major design parameters are the wavelength sensitivity, resolution, and dynamic range of the recording medium. Kodak Linagraph direct print paper, Polaroid high speed black and white film, and Dupont Dylux Instant Image Proof Paper[13] are commonly used to diagnose errors in beam alignment, but their low resolution and low dynamic range preclude accurate sensitometric analysis. Solid impressions of the intensity profile, formed in thermally deformable plastics, are used as diagnostic tools for high average power lasers. When the demagnification of a large diameter beam is possible, image tubes and detector arrays are available recording devices.

The photographic method is possibly the best near-field intensity recording technique. The wavelength sensitivity ranges from being adequate in the near infrared to overly responsive at ultraviolet wavelengths. The dynamic range can vary from less than two orders of magnitude to more than three orders of magnitude, depending on the type of emulsion and the selected slope (gamma) of the density verses logarithm of the exposure (D-logE) curve. Lack of resolution rarely presents a problem for large diameter HPPL beams. Accurate intensity values are obtained by generating D-log(E) curves for each combination of wavelength, pulsewidth, and development procedure.

Photographic methods are also available for the recording of far-field and equivalent-target-plane (ETP) intensity distributions. The equivalent plane camera produces a two-dimensional array of successive quasi-far-field images, each with a set of decreasing exposure levels.[14] Figure 2.6 illustrates the set-up necessary to obtain the

2-DIMENSIONAL ARRAY CAMERA

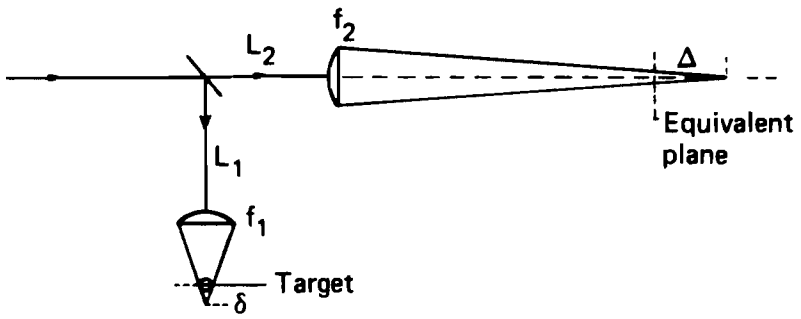

$$\Delta = \frac{f_2^2\,\delta}{f_1^2 - (L_2 - L_1)\,\delta + (f_2 - f_1)\,\delta}$$

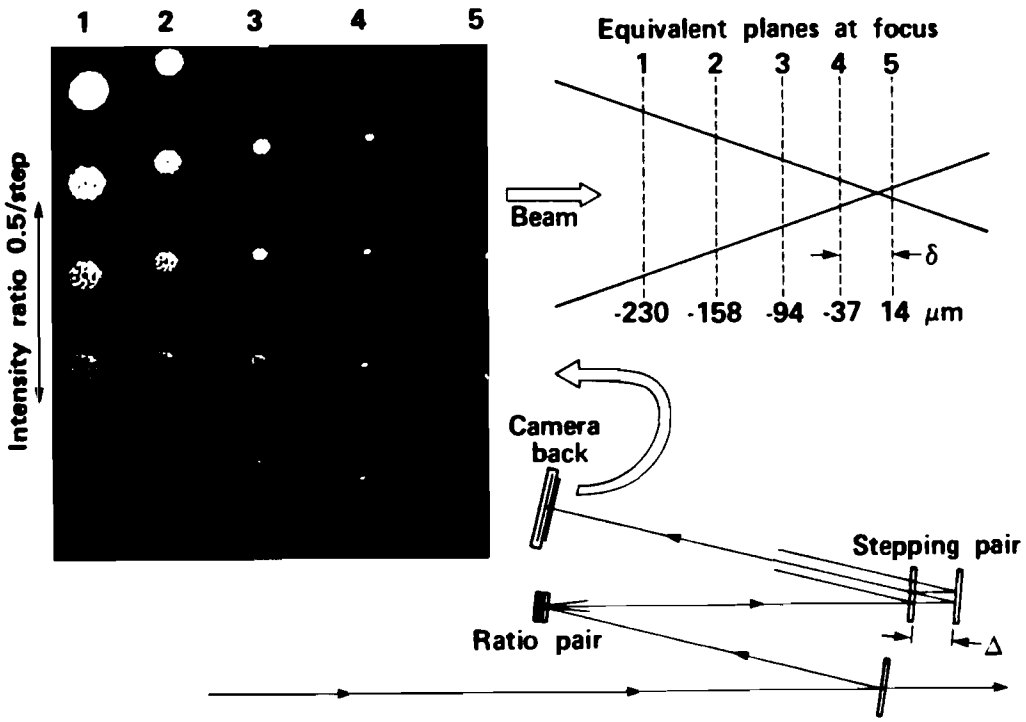

FIGURE 2-6

array. An energy reduction in the beam, along with the use of a long focal length lens, delivers the correct energy density to the film plane. Attenuating and narrow pass blocking filters are placed just before the film plane. All optics prior to the camera must be diffraction limited in quality, while the filters need only be locally homogeneous and uniformly transmitting.

It is generally accepted that ETP photographic methods are accurate when the plane is sufficiently removed from the focal plane. However, these methods can give misleading results and errors in energy density determinations when used near the focal plane of the lens.[15] If the intensity distribution has a spike in the center with broad wings of intensity below the film threshold, then this method yields a smaller than true image size. This is actually a problem of limited dynamic range and can apply to electronic detection as well. The array camera can offer a way to determine the extent of this problem for a given wavefront. By allowing the first few row elements of each focal column to be overexposed, large changes in image size due to this effect could be observed, and would indicate that the recording plane is too near focus for an accurate energy density calculation.

Pinhole methods were developed as a means of more accurately determining focal plane intensity distributions.[16] A single aperture is translated through a matrix of positions within the focal plane. A detector behind the aperture measures the energy of each laser pulse, one pulse per matrix element. The requirement of simultaneous measurements led to the development of pinhole methods that utilize the multiple side orders of a diffraction grating.[17]

Image tubes and detector arrays are available for single shot measurement of far-field intensity distributions. The vidicon tube has been used to image a CO_2 HPPL off diffusing surfaces.[18] The low resolution of 15 lines/mm and a dynamic range of less than two orders of magnitude make the vidicon tube inadequate for accurate measurements. Other image tubes with better performance are available but have not been tested on a HPPL.[19]

Pyroelectric arrays offer many advantages to wavefront measurement. (Pyroelectricity is the phenomenon by which crystals convert changes in temperature to electricity.[20]) Their flat spectral response and wide dynamic range make them an excellent choice of detector. The disadvantages include both a limited resolution and relatively high expense.

The CID (Charge Injection Device) imaging array offers superior resolution as well as a dynamic range of greater than five orders of magnitude.[21] The two-dimensional array consists of coupled metal-oxide silicon (MOS) capacitors which collect and store the photogenerated charge. Coincident X-Y selection is used to inject the stored charge into the bulk silicon. The output signal is related to the time integrated charging current to the MOS capacitor plates. The major disadvantage is system expense and, like the pyroelectric array, an accidental excess of energy, beyond the damage threshold of the material, results in costly repairs.

2.4 Conclusions

A technique which inherently can produce the far-field and near-field intensity distributions, as well as the near-field phase distribution of a HPPL most deserves investigation. The basic design of a system that has this capability is shown in Fig. 2.7.

The heart of this system is a holographic interferometer. The incident wavefront is split into an object beam and a newly created reference beam. Several techniques can be employed to create a suitable reference beam, which are discussed in Chapter Three. The two beams recombine at the holographic plate to form an interference pattern that is characteristic of both the object and the reference beams. A CW laser, operating at the same wavelength, can be used with the same set-up to reconstruct the object wavefront. This design takes advantage of the fact that holographic interferometry is capable of recording all of the information necessary for the complete recovery of the original complex amplitude distribution.

Various wavefront measurement techniques, considered impractical for use on the HPPL, are possible with a CW reconstruction of the same HPPL wavefront. A near-field intensity pattern could be appropriately demagnified and observed with a detector array without the risk of costly damages. The propagation of a CW plane wave along the path of the initial object beam would produce two beam inteferometric fringes, characteristic of the original phasefront. Furthermore, a typical PDI, designed for use with a CW laser, could be used in place of the separate-plane-wave reference scheme to allow the phasefront measurement to include the performance of the final focussing lens. While the reconstructed wavefront is still focussed through the lens, the PDI could be removed to observe a continuum of ETP images, and the far-field intensity

HOLOGRAPHIC INTERFEROMETER

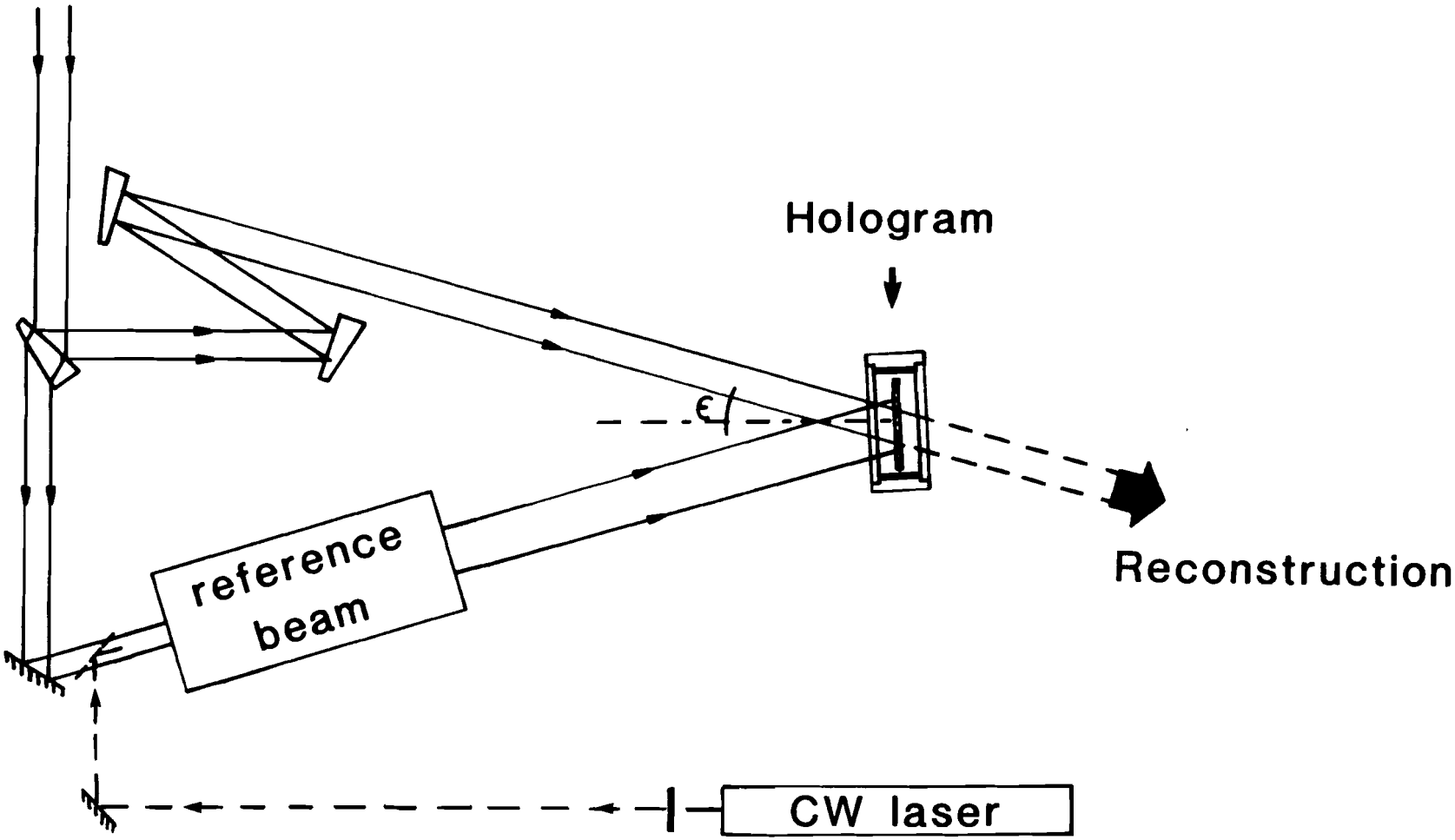

FIGURE 2-7

pattern could be mapped out over a curved surface corresponding to a spherical target. Additionally, this technique could reduce the difficulty associated with measuring the intensity distribution right at the focal plane.

Alternatively, phase measurements could be obtained without the use of an interferometer. A technique which utilizes acousto-optic modulation, heterodyne detection, and two-dimensional raster scanning has been developed to characterize laser beam quality.[22] This technique offers the ability to simultaneously measure the two dimensional phase and intensity distributions of the CW reconstruction of the pulsed beam.

In summary, the holographic interferometer inherently offers total wavefront storage. Various wavefront measurement techniques are better suited to a CW reconstruction of the HPPL. This design merits investigation since it offers both interferometric and intensity measurement capabilities not presently available for HPPL beam analysis.

REFERENCES

1. D. Malacara, Optical Shop Testing, John Whiley and Sons Inc., 1978, p.105

2. J.C. Wyant, "Double Frequency Lateral Shear Interferometer", Applied Optics, Sept. 1973, p. 2057

3. J.C. Wyant, Optical Testing and Testing Instrumentation, The Institute of Optics Contemporary Optics Notes

4. M.P. Rimmer and J.C. Wyant, "Evaluation of Large Aberrations Using a Lateral-Shear Interferometer Having Variable Shear", Applied Optics, Jan. 1975, p. 142

5. R. Hopkins, Laboratory for Laser Energetics, Unpublished Internal Report, June 11, 1982

6. S. Kumpan, Laboratory for Laser Energetics, Preliminary Internal Report, June 5, 1981

7. W.P. Linnick,"A Simple Interferometer for the Investigation of Optical Systems", C.R. Acad. Sci. URSS., Vol. 5, p.210, 1933

8. R.N. Smartt and J. Strong, Journal of Scientific Applications, 62, p. 737, 1972

9. V.K. Viswanathan, R.B. Hammond, I. Liberman, B.D. Seery, A. Gibbs and P.D. Bolen, Los Alamos Conference in Optics, April 1981

10. T. Miyamoto and K. Yasuura,"Measurements of Beam Parameters of a Laser Beam and its Diffraction Field, Using a Hologram", Applied Optics, Jan. 1971, p. 161

11. C. Roychoudhuri and B.J. Thompson,"Studying Beam Parameters of a Pulse Using Holography in Conjunction with Interferometry", Abstract Only, JOSA, 1972, p. 1357

12. H.J. Caufield, Handbook of Optical Holography, Academic Press, 1979, p. 219

13. M.W. Taylor, J.Goldhar and J.R. Murray, "An Instant Image Photographic Material Suitable for Ultraviolet Laser Beam Intensity", Lawrence Livermore Laboratory, June 14,1981

REFERENCES(continued)

14. H.G. Ahlstrom, Physics of Laser Fusion, Vol.II, Lawrence Livermore Laboratory, Jan. 1982

15. P.J. Shayler, "Laser Beam Distribution in the Focal Region", Applied Optics, Sept., 1978, p. 2673

16. B.J. Brannon, et. al., "Laser Focal Spot Measurements", Journal of Applied Physics, Aug. 1975, p. 3576

17. R.W. O'Neil, et. al., "Beam Diagnostics for High Energy Pulsed CO_2 Lasers", Applied Optics, Feb, 1974, p. 314

18. S. Mersch, J.S. Harris and D.L. Mullen, "Imaging CO_2 High Energy Laser Pulses with a Pyroelectric Vidicon Camera", Optical Engineering, May/June 1981

19. R.C.A., Electro-Optics Handbook, 1974, p. 173

20. C.B. Roundy, "Pyroelectric Arrays Make Beam Imaging Easy", Laser & Applications, Jan. 1983

21. General Electric, "Solid State Video/Digital Camera", 1981

22. C.P. Wang, "A New Technique for Measuring Two-Dimensional Laser-Beam Phase and Intensity Profiles", The Aerospace Corporation, Nov. 1983

III. THEORETICAL CONSIDERATIONS

3.1 Introduction

Holography is a method of recording and reconstructing the complex amplitude of a wavefront. The interference pattern between an object wavefront and a coherent reference beam is recorded. The use of a silver halide emulsion as an energy recording medium requires chemical processing in order to manifest the wavefront modulation. Wavefront reconstruction takes place, in a third step, when the hologram is illuminated with a second reference wave. Under certain conditions, the reconstructed wavefront is identical in form to the original wavefront, and may be operated upon as if it were the original. Other radiation characteristics, such as spectral bandwidth, pulsewidth, and polarization are not preserved. This chapter deals with the theoretical concepts which outline the requirements for an accurate wavefront recording of a High Peak Power Laser (HPPL), and an accurate, continuous wave reconstruction of the same wavefront.

3.2 Wavefront Recording

Communication theory offers insight into the relationship between heterodyne techniques and general holographic methods. Expressions describing the interference and modulation between the object wave and the reference wave (local oscillator) offer a clear understanding of the effects due to temporal variations, and show the means by which the amplitude and relative phase information are preserved. The following notation follows closely to Cathey.[1] Let the object wave and local oscillator (LO) wave be represented, respectively, by

$$\text{(Object)} \quad O(x,y)\cos[-\omega_1 t + \alpha x + \gamma z + \psi(x,y)] \tag{3-1}$$

$$\text{(LO)} \quad R(x,y)\cos[-\omega_2 t + \delta x + \mu z + \phi(x,y)] \tag{3-2}$$

where $O(x,y)$, $\psi(x,y)$ and $R(x,y)$, $\phi(x,y)$ represent the amplitude and phase distribution pairs of the object and LO waves, respectively. Plane polarization along the y axis is tacitly assumed. The relationships between the incident angles, χ and θ, and the pairs of propagation constants, α, γ, and δ, μ, of the object wave and LO, respectively, are illustrated in Fig. 3-1. The lines represent surfaces of constant phase, called phasefronts. The temporal frequencies, ω_1 and ω_2 of the object and LO waves, respectively, have units of radians/second. Square law detection of the interference signal between these two waves would produce a signal described by:

RECORDING GEOMETRY

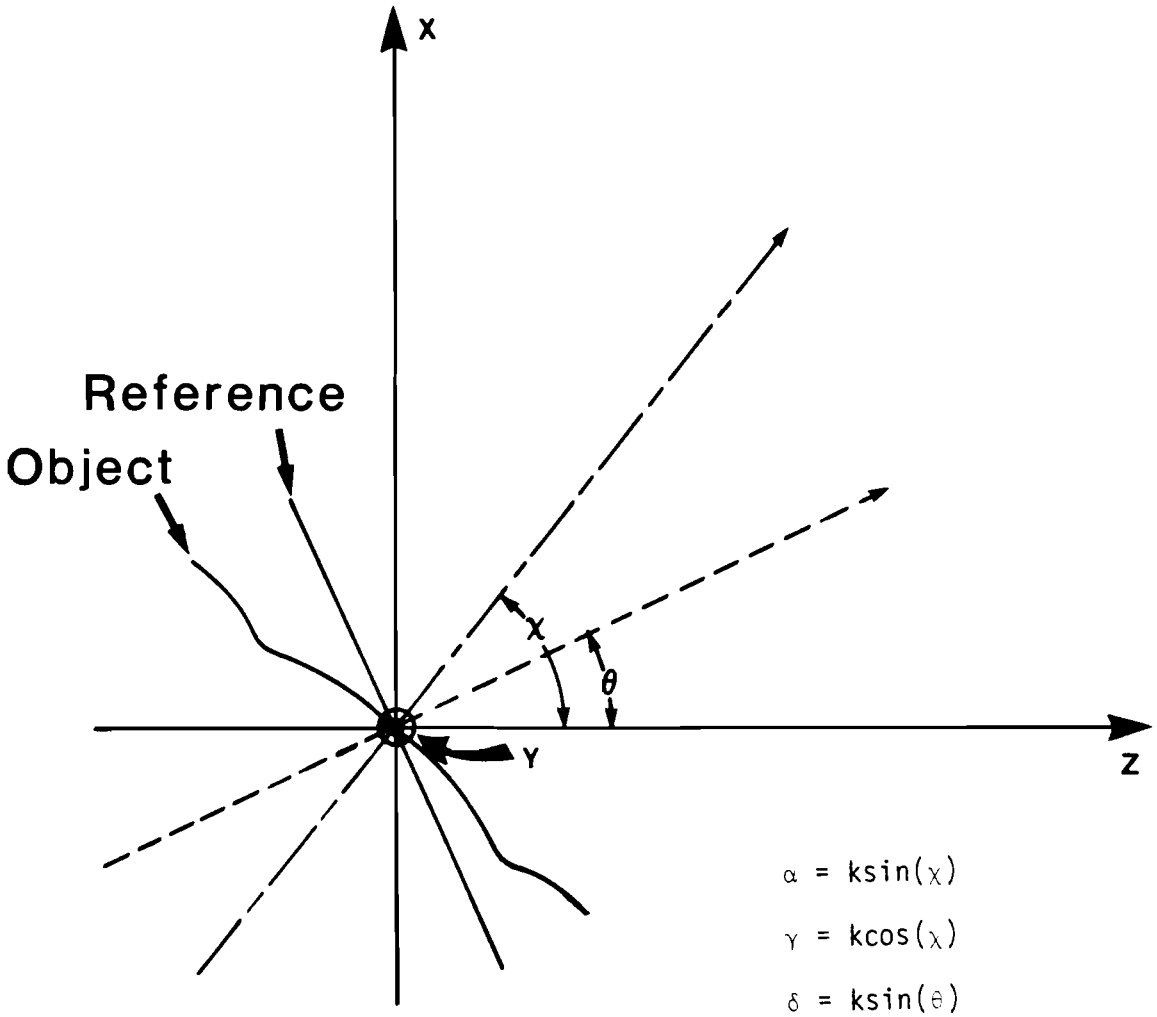

FIGURE 3-1

$$S(x,y,t) \propto O^2(x,y)/2 + O^2(x,y)\cos[-2\omega_1 t + 2\alpha x + 2\gamma z + \psi(x,y)]$$
$$+ R^2(x,y)/2 + R^2(x,y)\cos[-2\omega_2 t + 2\delta x + 2\mu z + \phi(x,y)]$$
$$+ O(x,y)R(x,y)\cos[-(\omega_1+\omega_2)t + (\alpha+\delta)x + (\gamma+\mu)z + \psi(x,y) + \phi(x,y)]$$
$$+ O(x,y)R(x,y)\cos[-(\omega_1-\omega_2)t + (\alpha-\delta)x + (\gamma-\mu)z + \psi(x,y) - \phi(x,y)]$$

(3-3)

The double frequency and sum frequency components vary too rapidly, for a detector with limited resolution and time response to record, leaving only the zero frequency and difference frequency terms,

$$S(x,y,t) \propto O^2(x,y)/2 + R^2(x,y)/2 + O(x,y)R(x,y) \cdot$$
$$\cos[-(\omega_1-\omega_2)t + (\alpha-\delta)x + (\gamma-\mu)z + \psi(x,y) + \phi(x,y)] \quad (3-4)$$

The original amplitudes and phases are linearly preserved in the cross terms. Heterodyning techniques utilize the intermediate frequency $\omega_{IF} = \omega_1 - \omega_2$ to reconstruct the object wave. Off-axis holographic methods utilize a spatial carrier frequency, and are referred to as Leith-Upatnieks holograms. Letting $\omega_1 = \omega_2$ and restricting the recording geometry to symmetrical illumination, $\theta = -\chi$, the expression becomes,

$$S(x,y) \propto O^2(x,y)/2 + R^2(x,y)/2 + O(x,y)R(x,y)\cos[2\alpha x + \psi(x,y) - \phi(x,y)]$$

(3-5)

Equation 3-5 shows that the amplitude distribution is recorded as an amplitude modulation of the spatial carrier frequency. The phase distribution is recorded as a phase modulation of the same carrier. A holographic recording of two nominally plane waves can be considered a modulated diffraction grating. The amplitude of the grating is influenced by the object amplitude, and the positions of the grating lines by the phase. Figure 3-2 illustrates each case, with 3-2a showing the sinusoidal variation of fringes due to the interference between two perfectly plane waves. If the object wave has only amplitude variations, such that $O(x,y) \neq$ constant and $\psi(x,y)$=constant, then only the intensity of the fringes varies (Fig. 3-2b). A phase modulation of a wave, such as $O(x,y)$=constant and $\psi(x,y) \neq 0$ causes a shift of the fringes and a change in their spacing (Fig. 3-2c).

Many materials are available to record and preserve the modulated wavefronts; dichromated gelatins, ferroelectric crystals, thermoplastics, photoresists, photochromic materials, and others are described in the literature. The most common medium, the silver halide emulsion, is discussed in most holographic references, and is well characterized by both the manufacturers and the scientific community. In the first phase of the holographic process, the wavefront information is recorded and preserved in the form of a latent image. The materialization of the wavefront modulation occurs during subsequent processing of the emulsion.

Development of the silver halide emulsion converts the latent image distribution to a metallic silver distribution, such that the macroscopic number density is proportional to the incident electric field squared. Referring to equation 3-5, we can describe the density distribution with the following equation,

MODULATED DIFFRACTION GRATING

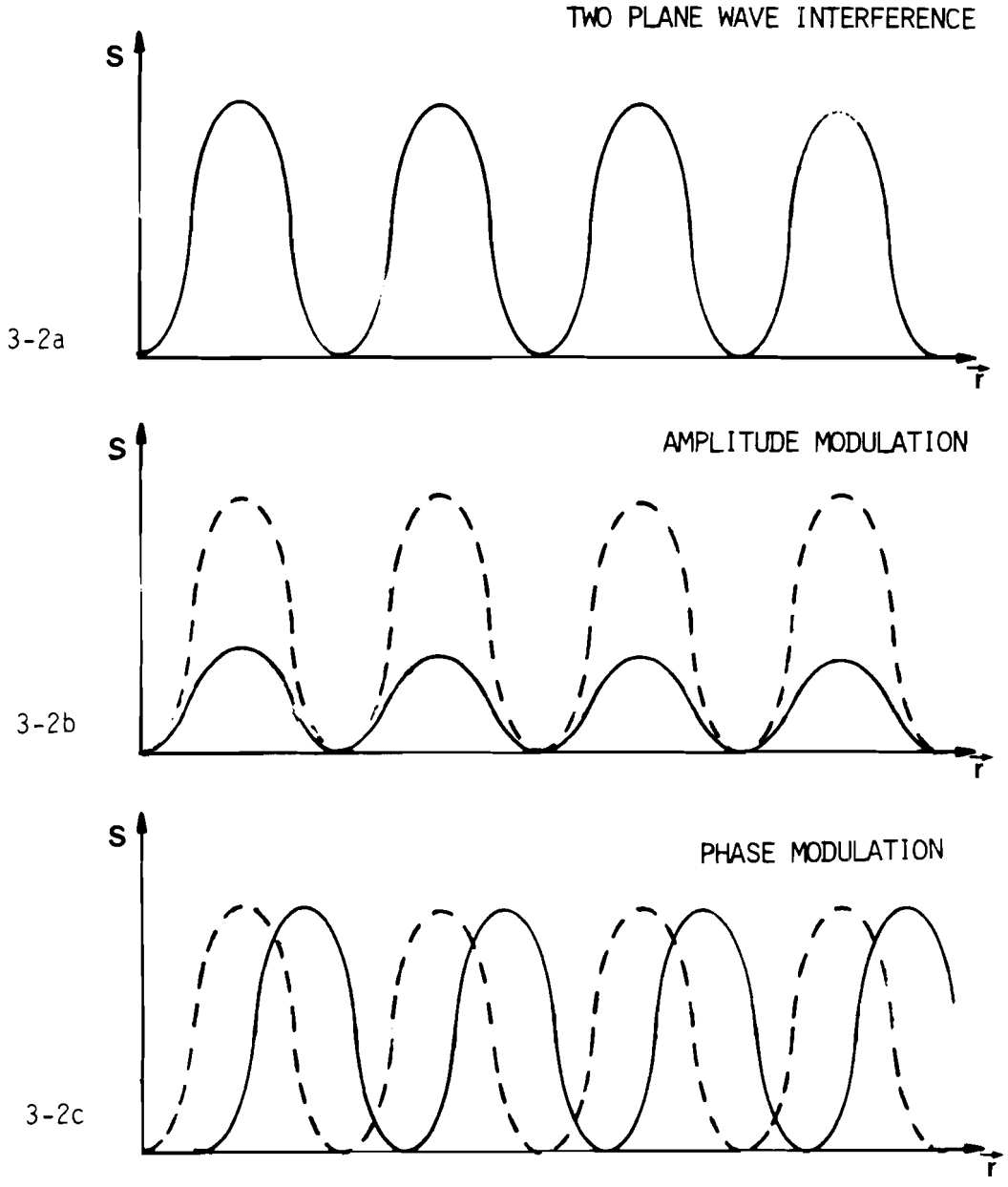

FIGURE 3-2

$$N(x,y) = N_0 + N_1\cos[2\alpha x + \psi(x,y) - \phi(x,y)] \tag{3-6}$$

Ideally, both the object and reference wavefronts are nearly plane waves, such that the difference between their phase distributions is a constant, i.e., $\psi(x,y) - \phi(x,y) = C$. For two plane waves we have,

$$N(x,y) = N_0 + N_1\cos[2(k\sin\chi)x + C] \tag{3-7}$$

where 2χ is the full angle between the plane waves. Planes of metallic silver appear after development as shown in Fig. 3-3. The equiphase planes satisfy the vector equation,

$$(\vec{k}_1 - \vec{k}_2) \cdot \Delta\vec{r} = 0 \tag{3-8}$$

The planes are separated by a distance d, where d is given by the Bragg condition:

$$d = \frac{\lambda_o}{2\sin(\chi)} = \frac{\lambda_{o/n}}{2\sin(\chi')} \tag{3-9}$$

As an example, let λ =351 nanometers and 2χ = 15°. The spatial frequency, $\nu = 1/d$, of the planes along the x-axis is 744 cycles per millimeter.

METALLIC SILVER DISTRIBUTION

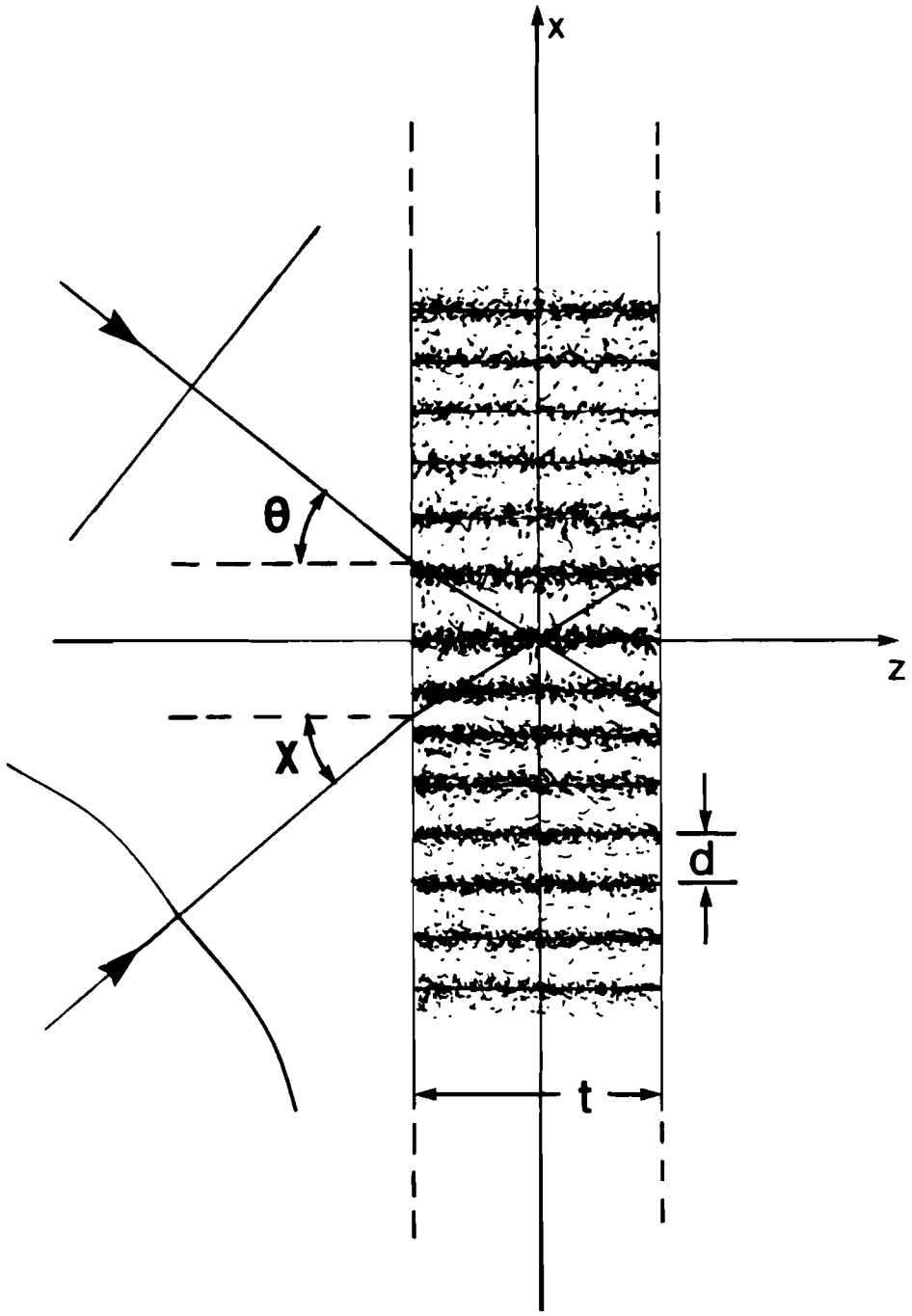

FIGURE 3-3

As the thickness of the photographic emulsion decreases, the planes of metallic silver approach rulings like that of a diffraction grating. A Q factor is defined to determine whether a certain combination of wavelength, emulsion thickness (t), and grating/plane separation will exhibit plane diffraction or volume diffraction characteristics.

$$Q = \frac{2\pi\lambda_o t}{nd^2} \tag{3-10}$$

Generally, a $Q > 10$ indicates a thick hologram, but volume effects are observed for $1 < Q < 10$.[3] Consider a continuation of the above example (λ = 351 nm, $2\chi = 15°$), where the emulsion thickness is seven microns, corresponding to an Agfa-Gevaert 10E56 holographic plate. Substituting the expression for the plane spacing, d, into equation 3-10 yields a calculated Q factor of,

$$Q = \frac{8\pi t \sin^2(\chi)}{n\lambda_o} \simeq 6 \tag{3-11}$$

Although plane diffraction theory sufficiently describes the reconstruction process, volume effects are anticipated during holographic experiments which utilize the A-G 10E56 plate.

The materialization of the wavefront modulation occurs during development of the silver halide emulsion, and continues throughout subsequent processing. The amplitude transmittance of a photographic negative that is illuminated by a plane wave of amplitude $C_o(x)$, is given by

$$T_A(x) = C_0(x)e^{-a(x)t}\, e^{ikn(x)t(x)} \qquad (3\text{-}12)$$

where $a(x)$ = absorption constant
$t(x)$ = emulsion thickness
$n(x)$ = refractive index

If the exposure and development cause a spatial variation of the absorption constant, then the transmitted amplitude is modulated in accordance with the exposure and an amplitude hologram is said to exist. Furthermore, if the exposure and development cause a spatial variation in the emulsion thickness, or the refractive index, then a phase hologram also exists.

The metallic silver rulings give rise to an amplitude hologram, but a complex transmittance, due to a phase modulation, from a surface relief and from index variations in the emulsion, is usually observed.[1] We will concentrate on the amplitude hologram and consider phase modulation as a source of coherent noise.

Frieser's two step model (Fig. 3-4) illustrates the transfer from exposure to density.[4] Step one shows the lowered modulation of the signal, characteristic of a modulation transfer function (MTF) less than one, for a given spatial frequency. For the case of two plane wave interference, only a narrow range of spatial frequencies need to be recorded, and the MTF is approximately constant over this range. Step two shows the transfer from effective exposure (E) to density (D). Since the amplitude transmission is related to the density in the following way,

AMPLITUDE TRANSFER CHARACTERISTIC CURVES

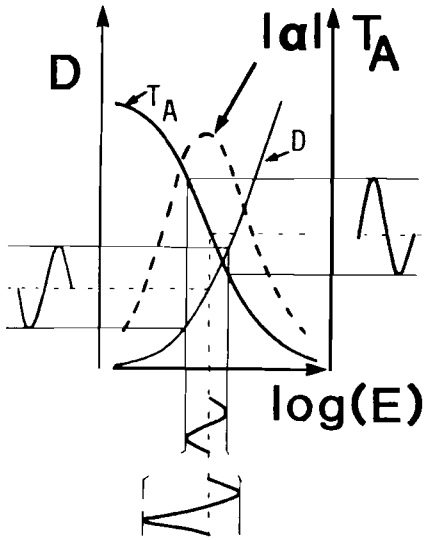

Frieser's Model

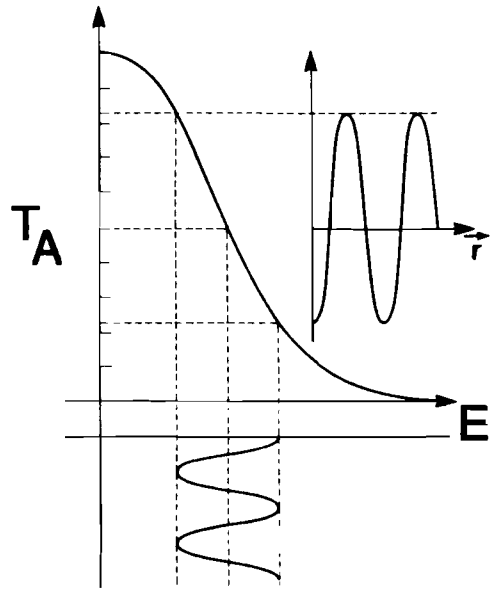

T_A–log(E)

FIGURE 3-4